# Measuring and modeling the dissolution of nonideally shaped dense nonaqueous phase liquid pools in saturated porous media

**ARTICLE** *in* WATER RESOURCES RESEARCH · AUGUST 2002

Impact Factor: 3.71 · DOI: 10.1029/2001WR000444



**3 AUTHORS**, INCLUDING:

Thomas C. Harmon
University of California, Merced
**90** PUBLICATIONS **1,032** CITATIONS

SEE PROFILE

Constantinos V. Chrysikopoulos
Technical University of Crete
**143** PUBLICATIONS **1,994** CITATIONS

SEE PROFILE

# Measuring and modeling the dissolution of nonideally shaped dense nonaqueous phase liquid pools in saturated porous media

Brian K. Dela Barre[1] and Thomas C. Harmon

Department of Civil and Environmental Engineering, University of California, Los Angeles, California, USA

Constantinos V. Chrysikopoulos

Department of Civil and Environmental Engineering, University of California, Irvine, California, USA

Received 23 February 2001; revised 16 February 2002; accepted 4 March 2002; published 3 August 2002.

[1] A three-dimensional physical aquifer model was used to study the dissolution of a dense nonaqueous phase liquid (DNAPL) pool. The model aquifer comprised a packing of homogeneous, medium-sized sand and conveyed steady, unidirectional flow. Tetrachloroethene (PCE) pools were introduced within model aquifers atop glass- and clay-lined aquifer bottoms. Transient breakthrough at an interstitial velocity of 7.2 cm/h, and three-dimensional steady state concentration distributions at velocities ranging from 0.4 to 7.2 cm/h were monitored over periods of 59 and 71 days for the glass- and clay-bottom experiments, respectively. Pool-averaged mass transfer coefficients were obtained from the observations via a single-parameter fit using an analytical model formulated with a second type boundary condition to describe pool dissolution [*Chrysikopoulos*, 1995]. Other model parameters (interstitial velocity, longitudinal and transverse dispersion coefficients, and pool geometry) were estimated independently. Simulated and observed dissolution behavior agreed well, except for locations relatively close to the pool or the glass-bottom plate. Estimated mass transfer coefficients ranged from 0.15 to 0.22 cm/h, increasing weakly with velocity toward a limiting value. Pool mass depletions of 31 and 43% for the glass- and clay-bottom experiments failed to produce observable changes in the plumes and suggested that changes in pool interfacial area over the period of the experiment were negligible. Dimensionless mass transfer behavior was quantified using a modified Sherwood number ($Sh^*$). Observed $Sh^*$ values were found to be about 2–3 times greater than values predicted by an existing theoretical mass transfer correlation, and 3–4 times greater than those estimated previously for an ideally configured trichloroethene (TCE) pool (circular and smooth). It appeared that the analytical model's failure to account for pore-scale pool-water interfacial characteristics and larger scale pool shape irregularities biased the $Sh^*$ estimates toward greater values. *INDEX TERMS:* 1831 Hydrology: Groundwater quality; 1832 Hydrology: Groundwater transport; *KEYWORDS:* DNAPL, pool, dissolution, mass transfer, three-dimensional

## 1. Introduction

[2] Dense nonaqueous phase liquid (DNAPL) can act as a long-term source of groundwater contamination. The nature of a contaminant plume emanating from the DNAPL is a result of the interplay between dissolution at the DNAPL-water interface, the interfacial area and its availability to the flow regime, and advection-dispersion processes in heterogeneous porous media [*Miller et al.*, 1998; *Khachikian and Harmon*, 2000]. DNAPL entrapped in a porous medium is conventionally categorized as a distribution of residual ganglia or as pooled bodies. The latter occur when the pathway of a migrating DNAPL is impeded by a low permeability geologic unit. This research investigates the controlled dissolution of a pooled DNAPL.

[3] A body of theoretical work has shown that DNAPL pools have the potential to persist in the environment due to their relatively low surface-to-volume ratio [*Johnson and Pankow*, 1992; *Chrysikopoulos et al.*, 1994; *Chrysikopoulos*, 1995; *Holman and Javandel*, 1996; *Lee and Chrysikopoulos*, 1998; *Kim and Chrysikopoulos*, 1999]. Intermediate-scale box experiments [*Pfannkuch*, 1984; *Anderson et al.*, 1992; *Saba and Illangasekare*, 2000; *Chrysikopoulos et al.*, 2000] employing realistic DNAPL configurations have been used to link laboratory and field observations by providing controlled three-dimensional data sets for model testing. Early experimental work on pool dissolution qualitatively corroborates dissolution theory [*Chrysikopoulos et al.*, 1994; *Pearce et al.*, 1994; *Voudrias and Yeh*, 1994; *Whelan et al.*, 1994]. However, data from such experiments are relatively sparse and inadequate to conclusively quantify the dissolution rate from pools in three dimensions.

[4] The primary goal of this research is to observe the controlled dissolution of DNAPL pools into an overlying porous medium, and to quantify the longevity of such pools.

[1]Now at Tetra Tech EM Inc., Reno, Nevada, USA.


0043-1397/02/2001WR000444$09.00

Whenever DNAPL enters porous media, pore scale issues will play an important role in determining the DNAPL-water interfacial area and its availability to dissolution. Pore network model studies have examined the problem of dissolving residual NAPL in porous media and have begun to link multiphase flow theory with that for NAPL dissolution in one- and two-dimensional systems [*Reeves and Celia*, 1996; *Jia et al.*, 1999a, 1999b; *Schaefer et al.*, 2000; *Zhou et al.*, 2000; *Held and Celia*, 2001a]. Findings from this body of work imply that pore scale features of a DNAPL pool-water interface will impact dissolution and may change significantly as sufficient portions of the pool dissolve.

[5] A secondary objective of this work is to more rigorously test an existing mathematical model describing the dissolution of ideally shaped DNAPL pools with a 2nd type boundary condition [*Chrysikopoulos*, 1995]. This model was tested against concentration fields generated using an ideally configured trichloroethene (TCE) pool [*Chrysikopoulos et al.*, 2000], i.e., a pool experimentally controlled to preserve constant mass and shape, and perfectly aligned with the lower porous medium boundary (Figure 1a). Here, DNAPL pools were introduced atop impermeable (glass) and relatively impermeable (clay) surfaces at the bottom of a physical aquifer model (Figure 1b). In contrast to the previous study, these DNAPL pools were irregular in shape, finite in mass and resided within the experimental porous medium, where interfacial forces were allowed to affect the pool surface.

## 2. DNAPL Pool Dissolution Theory

[6] For a two-dimensional DNAPL pool (pool thickness is considered inconsequential relative to the thickness available for advective flow), the mass transfer coefficient varies in both the $x$ and $y$ directions along the interface. The local mass transfer coefficient has a maximum value at the upstream edge of the DNAPL pool and decreases with distance from the front end [*Chrysikopoulos and Lee*, 1998]. Under steady state physicochemical and hydrodynamic conditions, this distribution is independent of time. For a uniform DNAPL pool, it is possible to theoretically estimate the local mass transfer coefficient at the DNAPL-water interface [*Chrysikopoulos and Kim*, 2000] as well as the average mass transfer coefficient [*Kim and Chrysikopoulos*, 1999]. The average mass transfer coefficient governing the dissolution flux from the entire pool is of greater practical interest for larger scale modeling efforts.

[7] Solute transport (after dissolution) in saturated homogeneous porous media under steady unidirectional flow is governed by the following equation

$$R\frac{\partial C(t,x,y,z)}{\partial t} = D_x\frac{\partial^2 C(t,x,y,z)}{\partial x^2} + D_y\frac{\partial^2 C(t,x,y,z)}{\partial y^2} + D_z\frac{\partial^2 C(t,x,y,z)}{\partial z^2} - U_x\frac{\partial C(t,x,y,z)}{\partial x} \quad (1)$$

where $C(t, x, y, z)$ is the liquid phase solute concentration; $x, y, z$ are the spatial coordinates in the longitudinal, lateral and vertical directions, respectively; $D_x$, $D_y$, $D_z$ are the longitudinal, lateral, and vertical hydrodynamic dispersion coefficients, respectively; $R$ is the dimensionless retardation factor; and $U_x$ is the average interstitial fluid velocity in the longitudinal direction.

[8] The DNAPL pool dissolution process can be modeled using boundary layer theory [*Chrysikopoulos*, 1995]:

$$\mathbf{D}_e\frac{\partial C(t,x,y,0)}{\partial z} = k(t,x,y)[C_s - C(t,x,y,\infty)], \quad (2)$$

where $\mathbf{D}_e = \mathbf{D}/\tau^*$ is the effective molecular diffusion coefficient; D is the molecular diffusion coefficient; $\tau^*$ is the tortuosity factor ($\tau^* \geq 1$); $k(t,x,y)$ is the local mass transfer coefficient; $C_s$ is the aqueous solubility and $C(t,x,y,\infty) = 0$ because it corresponds to the contaminant concentration outside the boundary layer. It is assumed here that the pool thickness is insignificant relative to the aquifer thickness. The complete set of initial and boundary conditions appropriate for the model aquifer system are as follows:

$$C(0,x,y,z) = 0, \quad (3)$$

$$C(t,\pm\infty,y,z) = 0, \quad (4)$$

$$C(t,x,\pm\infty,z) = 0, \quad (5)$$

$$\mathbf{D}_e\frac{\partial C(t,x,y,0)}{\partial z} = \begin{cases} -k^*C_s & (x-\ell_{x_0})^2+(y-\ell_{y_0})^2 \leq r_p^2, \\ 0 & (x-\ell_{x_0})^2+(y-\ell_{y_0})^2 > r_p^2, \end{cases} \quad (6)$$

$$C(t,x,y,\infty) = 0, \quad (7)$$

where $\ell_{x_0}$ and $\ell_{y_0}$ are the pool center's coordinates, and $r_p$ is the radius of the circular pool. The pool boundary condition employed here assumes that the DNAPL-water interface for the pool is smooth, with an area ($A_{nw}$) defined simply by its radius ($A_{nw} = \pi r_p^2$). A model formulation addressing interfacial phenomena would be required to better define the effective pool surface area. In the present formulation, additional surface area in the form of capillary-induced curvature could be accounted for indirectly by increasing the mass transfer coefficient. It should be noted that the boundary condition outside the pool at $z = 0$ is a zero flux boundary ($dC/dz = 0$). For steady state conditions, $k(t,x,y)$ becomes constant in time ($\hat{k}(x, y)$). This local parameter was replaced in equation (6) by the spatially averaged mass transfer coefficient, $k^*$,

$$k^* = \frac{1}{A}\int_A \hat{k}(x,y)dA \quad (8)$$

which is more useful for macroscopic modeling purposes.

## 3. Physical Aquifer Model System and Sampling Protocols

### 3.1. Intermediate-Scale Model Aquifer System

[9] A 150 × 50 × 35 cm tank with 1.27 cm thick glass walls and bottom contained the model aquifer used in this investigation (Figure 1). Framed stainless steel screening (#80 US Std. Mesh size) was used to fabricate clear wells at the influent and effluent ends of the tank. Pumping maintained a constant head difference between the clear wells. The pump employed (Masterflex Model 7420, Cole-Parmer,

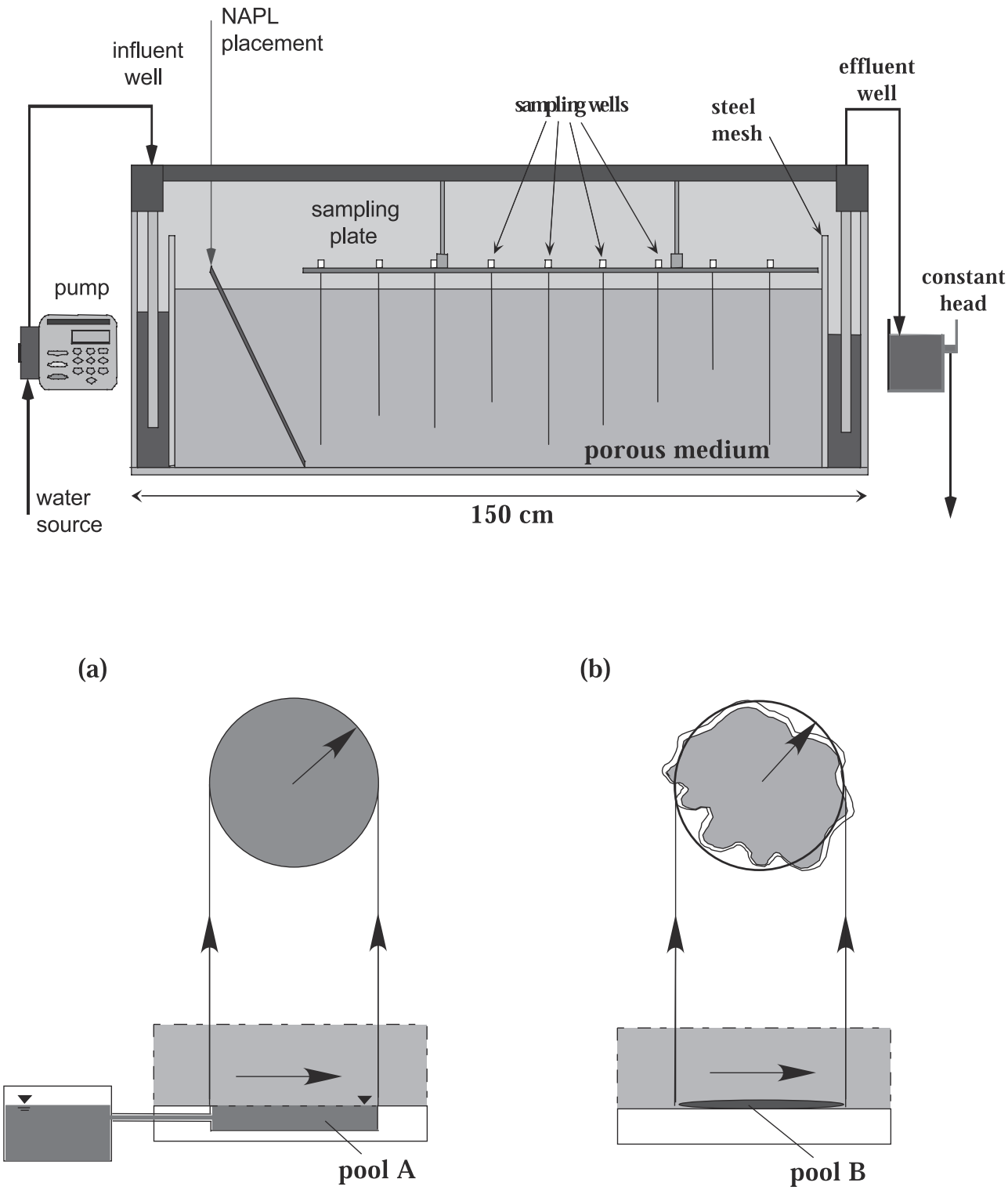


**Figure 1.** Schematic profile of the physical aquifer model showing flow control mechanism, DNAPL pool placement tube and variable level sampling locations (see Figure 2 for actual three-dimensional sampling point layout). Details of pool configurations are for (a) ideally shaped and leveled pool employed by *Chrysikopoulos et al.* [2000] and (b) the pool employed in this work (actual shape).

Vernon Hills, Illinois) operated at flow rates ranging from 0.035 to 35 mL/min. These flow rates yielded an interstitial velocity range of 0.3 to 10 cm/h, (17 to 0.5 days, respectively, for the passage of a pore volume). The entire system was housed in an environmental chamber maintained at 15 ± 0.1°C. The effluent clear well water elevation was maintained using an external constant head reservoir and weir system. Ultrapure water from a NANOpure polishing unit with ROpure pretreatment (Barnstead/Thermolyne, Dubuque, IA) was used.

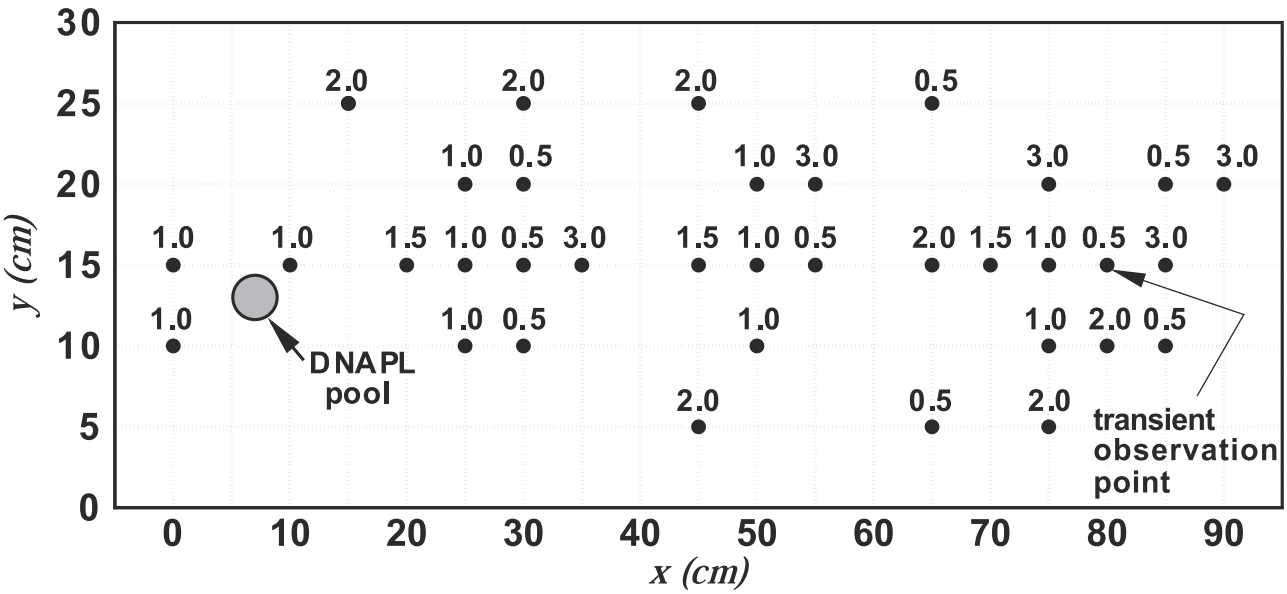


**Figure 2.** Plan view of the model aquifer sampling plate showing active sampling locations in terms of the coordinate system used in the simulations. The numbers denote the elevation ($z$ coordinate) of the sampling point above the aquifer bottom.

[10] Two packing configurations were employed: homogeneous sand supported by the glass tank-bottom and the same homogeneous sand supported by a clay layer. The material employed to fabricate the aquifer was #60 Lonestar sand (U.S. std. sieve size, Lonestar Sand, Monterey, CA). Grain sizes larger than about 0.425 mm (#40 U.S. Std. Sieve) were removed prior to packing. The geometric mean grain diameter of the resulting sand was 0.33 mm. The clay material comprised a pliable mixture of montmorillonite, kaolinite and smectite placed and leveled in a 1-cm thick layer along the tank bottom. For both the glass- and clay-bottom experiments, the sand was placed in 2–3 cm lifts under a water head of approximately 5–10 cm to a total packing depth of 20 cm. This configuration resulted in a packed volume of about 115,200 $cm^3$ (120 × 48 × 20 cm). The tank was then filled with water (several cm above the upper level of packing) and left overnight to settle and saturate. Following this initial saturation, the media was physically agitated by inserting a mechanically vibrated, 5 mm diameter aluminum rod on 5 cm intervals. The final porosity of the model aquifer was determined to be 0.38, and the bulk density was determined to be 1.60 $g/cm^3$. The water level stabilized to an average saturated depth of 13 cm. The system was then flushed at maximum velocity until the effluent clear well was free of suspended fine material.

[11] A Plexiglas grid of potential well locations anchored immediately above the porous medium fixed the horizontal location of sampling needles in terms of the coordinate system assigned for modeling purposes (Figure 2). Thirty-five observation ports were installed in the experimental aquifer to allow periodic sampling of concentrations resulting from tracer injection or pool dissolution. Each port consisted of a 20-gauge stainless steel needle (0.58 mm inner diameter, Hamilton Syringe, Reno, Nevada) guided through holes in the support grid and anchored to the surface. Wire inserted in the needle during the placement process prevented clogging. The sampling points were fixed at elevations ranging from 0.5 to 3.0 cm above the glass or clay aquifer bottoms as designated in Figure 2. These elevations were selected on the basis of preliminary model simulations using reasonable parameter estimates [*Lee and Chrysikopoulos*, 1998; *Kim and Chrysikopoulos*, 1999], and on the practical detection limits for organic solutes (discussed below). A small stream of 200 mg/L sodium azide solution was introduced to the influent clear well to inhibit biological growth.

### 3.2. Estimating Hydrodynamic Dispersion and Sorption Parameters

[12] Model sensitivity analysis for one-dimensional systems has demonstrated that the effluent concentrations are insensitive to dispersivity values in the range of 0.01 to 1 cm [*Powers et al.*, 1991; *Pennell et al.*, 1993]. In multi-dimensional systems, dispersion plays a critical role in determining the shape of the plume emanating from a DNAPL. Thus, accurate estimates of mass transfer rate coefficients for DNAPL pools require accurate dispersion parameter estimates. Pulse-input tracer tests were used to quantify local interstitial velocities. A comparison of pulse travel times for different regions and elevations in the box verified that a uniform flow field had been achieved. Local horizontal velocity values were in agreement with the bulk interstitial velocity values estimated using the aquifer dimensions and flow rate. Preliminary tests demonstrated that the pulse-input tracer breakthrough curve shapes were easily biased by over-sampling, and therefore not useful for quantifying dispersion. Instead, dispersion coefficient values for the model aquifer were estimated using step-input breakthrough tracer tests. The stationary tail offers the advantage of being insensitive to sampling and highly sensitive to the transverse dispersion coefficients. The concentration front, which is not as susceptible to the sampling frequency problem as a pulse signal, is more sensitive to the longitudinal dispersion parameter.

**Table 1.** Summary of PCE Dissolution Model Parameter Estimates and Resulting Fitted Values of the Pool-Averaged Mass Transfer Coefficient ($k^*$)

| Parameter | Estimate[a] | Source of Estimate |
|---|---|---|
| $C_s$ | 180 ± 10 mg/L | batch measurement |
| $r_p$, glass bottom | 1.9 ± 0.1 cm | visual measurement |
| $r_p$, clay bottom | 2.5 ± 0.1 cm | clay depression size |
| D | 0.026 ± 0.002 cm$^2$/h | *Wilke and Chang* [1955] |
| $\tau^*$ | 1.7 ± 0.05 (dimensionless) | column diffusion experiments |
| $U_x$ | | |
| Slow | 0.4 ± 0.003 cm/h | pulse tracer tests; $Pe_x$ = 7.6, $Pe_y$ = 38 |
| Medium | 2.6 ± 0.005 | pulse tracer tests; $Pe_x$ = 8.5, $Pe_y$ = 71 |
| Fast | 7.2 ± 0.007 | pulse tracer tests; $Pe_x$ = 8.6, $Pe_y$ = 86 |
| Clay bottom | 5.6 ± 0.007 | pulse tracer tests; $Pe_x$ = 11.2, $Pe_y$ = 108 |
| $D_x$ | | |
| Low | 0.10 ± 0.008 cm$^2$/h | step tracer tests ($\alpha_L$ = 0.22 ± 0.02 cm) |
| Medium | 0.58 ± 0.05 | step tracer tests ($\alpha_L$ = 0.22 ± 0.02 cm) |
| High | 1.59 ± 0.14 | step tracer tests ($\alpha_L$ = 0.22 ± 0.02 cm) |
| Clay bottom | 1.25 ± 0.11 | step tracer tests ($\alpha_L$ = 0.22 ± 0.02 cm) |
| $D_y = D_z$ | | |
| Low | 0.02 ± 0.002 cm$^2$/h | step tracer tests ($\alpha_T$ = 0.02 ± 0.0015 cm) equation (16)[a] |
| Medium | 0.07 ± 0.005 | step tracer tests ($\alpha_T$ = 0.02 ± 0.0015 cm) equation (16)[a] |
| High | 0.16 ± 0.011 | step tracer tests ($\alpha_T$ = 0.02 ± 0.0015 cm) equation (16)[a] |
| Clay bottom | 0.13 ± 0.009 | step tracer tests ($\alpha_T$ = 0.02 ± 0.0015 cm) equation (16)[a] |
| $k^*$ | | |
| Low | 0.15 ± 0.02 cm/h | single-parameter fit to pool dissolution model[b] |
| Medium | 0.21 ± 0.03 | single-parameter fit to pool dissolution model[b] |
| High | 0.22 ± 0.04 | single-parameter fit to pool dissolution model[b] |
| Clay bottom | 0.21 ± 0.06 | single-parameter fit to pool dissolution model[b] |

[a] Error (±) bounds for parameters: $C_s$, standard deviation ($n$ = 6); $r_p$ visual estimate; $D$, relative error associated with Wilke-Chang expression (7.5%); $\tau^*$, 95% confidence interval (CI) for optimized parameter in fit to diffusion data [*Dela Barre*, 1999]; $U_x$, standard deviation ($n$ = 7 for each velocity). Dispersion coefficients were estimated using $D_i = \alpha_i U_x + D_e$ with error bounds estimated by propagating the error associated with the parameter estimates for dispersivity (95% CI for optimized parameter in fit to step input tracer data).

[b] Low-velocity $k^*$ estimate based on single data set of 28 observations; medium, high, and clay bottom $k^*$ estimates are each the average duplicate data sets of 14 observations. Error bound on $k^*$ estimates are based on fitting extremities achieved using minimum and maximum dispersion parameter values.

[13] Dispersion coefficients were determined by fitting the observed step breakthrough response to an advection-dispersion transport model for a conservative, nonsorbing solute in a homogeneous porous medium subject to unidirectional flow and three-dimensional dispersion [*Chrysikopoulos et al.*, 2000]. The fits were optimized by coupling the dispersion model solution to the parameter optimizing routine PEST [*Doherty et al.*, 1994]. PEST employs the maximum neighborhood approach [*Marquardt*, 1959, 1963], which combines steepest descent and the Gauss-Newton methods. Here, the longitudinal and transverse dispersion coefficients were fitted, assuming equal horizontal ($D_y$) and vertical ($D_z$) transverse contributions.

[14] The relatively low amount of dispersion observed in the tracer tests implied that the diffusive contribution was significant and required quantification. The tortuosity ($\tau^*$) value was estimated by monitoring the transport of a tracer (tritiated water) solute within the same sand-packing under quiescent conditions. The effective tortuosity factor for the relatively nonrestrictive interparticle pores associated with a well-sorted sand will be reasonably independent of the tracer molecule. Thus we chose to use tritiated water, as opposed to the solute of interest (PCE), because of the greater cost and safety concerns associated with carbon-14 labeled PCE. A one-dimensional diffusion column was fabricated using a brass sleeve (2.54 cm in diameter) situated atop a screened, well-stirred reservoir. The box-packing procedure described earlier was replicated in this system. A support apparatus was fabricated for anchoring a microsyringe to the diffusion column to facilitate the collection of 2 μL samples as a function of depth [*Dela Barre*, 1999]. Concentration profiles were measured at 7 and 21 days and modeled using the solution to the equation for diffusive transport from a source of limited volume into a semi-infinite column [*Crank*, 1975]. Results for both profiles collected yielded a tortuosity estimate of 1.7 for the tritiated water [*Dela Barre*, 1999], which is reasonable for a sandy medium [*Perkins and Johnston*, 1963]. Estimating an aqueous diffusivity (D) value of $7.1 \times 10^{-6}$ cm$^2$/s at 15°C for PCE [*Wilke and Chang*, 1955], and assuming the same tortuosity value for both solutes, the corresponding $D_e$ value for PCE is $4.2 \times 10^{-6}$ cm$^2$/s (0.015 cm$^2$/h).

[15] The dispersion parameters used to model DNAPL pool dissolution results are summarized in Table 1. To arrive at the values indicated, the fitted dispersion coefficients and effective diffusivity value from the tracer experiments were first used to estimate the porous medium dispersivity values ($\alpha_L$ = 0.22 and $\alpha_T$ = 0.02 cm) as per *Bear* [1972]. These dispersivity values are in good agreement with those obtained for a similar system [0.26 and 0.02 cm, *Chrysikopoulos et al.*, 2000]. Given these dispersivity values, dispersion coefficients were calculable for the interstitial velocities employed in the pool dissolution experiments.

[16] The PCE sorption capacity of the sand was determined in batch samples contained in flame-sealed ampules [*Ball and Roberts*, 1991; *Harmon and Roberts*, 1994]. Triplicate samples were equilibrated at each of five concentrations ranging from 1 mg/L to 50 mg/L. The resulting isotherm was described well by linear isotherm, and yielded a distribution coefficient ($K_d$) of 0.30 mL/g. This $K_d$ value corresponds to a retardation factor of approximately 2.3.

### 3.3. DNAPL Pool Placement and Organic Solute Sampling

[17] In the first experiment, a single DNAPL pool was placed on the glass tank-bottom by pumping pure tetrachloroethene (PCE) through a 0.3 mm (inner diameter) glass tube positioned during the packing procedure. In the second experiment, a PCE pool was placed in a 3 cm diameter depression on top of the clay layer. In both cases, the tube fully penetrated the porous medium, contacting the bottom surface at coordinates $x$ = 7, $y$ = 13 (Figure 2). Initially, the injection system was filled with water to prevent air-intrusion into the saturated media during placement. Pools were injected at a rate of about 6 mL/h while maintaining a constant interstitial velocity (0.4 cm/h). After approximately 1 mL (1.62 g) of PCE was placed at the bottom of the medium, the injection was halted and the tube was capped. For the case of the glass-bottom, capillary and gravitational forces caused the pool to spread laterally along the bottom of the tank in a roughly circular pattern. The visually observed pool outline was traced with indelible ink on the bottom of the glass tank (Figure 1b). The area of the pool shape was estimated to be about 11.3 ± 1.2 $cm^2$. This corresponds to a nominal diameter for a circular pool of 3.8 ± 0.2 cm, and implies a pool thickness of slightly more than 0.1 mm. For the case of the clay-bottom, the pool was not observable, and was assumed to be distributed evenly in the depression.

[18] For the glass-bottom experiment, the velocity was increased to 7.2 cm/h immediately after pool placement. Temporal sampling was carried out at the designated observation point (Figure 2) approximately 73 cm downgradient of the pool to determine when steady state dissolution conditions were achieved. Subsequent sampling was synoptic and occurred at 4.5 12, 17, 31 and 59 days for interstitial velocities of 7.2, 2.6, 7.2, 2.6 and 0.4 cm/h, respectively. For the clay-bottom experiment, synoptic sampling was undertaken 34 and 71 days after pool placement at a constant interstitial velocity of 5.6 cm/h. The additional time for the clay-bottom experiment was intended to allow for equilibration between the clay and the lower portions of the plume. All aqueous samples were collected using a 1 mL gas-tight syringe. Approximately 30 to 40 μL of aqueous solution were purged from each well immediately prior to sample collection. Sampling events began at downgradient well locations and proceeded toward the pool to minimize the effects of previous sample withdrawal on subsequent sampling events. For each sample, a 20 to 60 μL volume (determined gravimetrically) was withdrawn and delivered to a 2 mL glass receiving vial. The smaller volumes were taken near the centerline of the plume and deeper in the aquifer, where greater concentrations were expected. The larger volumes were collected on the periphery and at higher elevations. The entire system was allowed to recover for the passage of two to three pore volumes prior to subsequent sampling events.

[19] Samples from the model aquifer were prepared for analysis using a micro-extraction protocol developed to accommodate the limited sample volumes available in these experiments. Receiver vials contained 1.0 to 1.8 mL of pentane spiked with an internal standard (1-bromo, 2-chloro-propane). Specific volumes were inversely related to the magnitude of the anticipated solute concentration. Samples were dispensed below the surface of the extracting solvent to minimize volatilization losses. Prior to analysis, the pentane phase was transferred from the receiver vial to a micro-vial and capped using a crimped foil cap with Teflon/silicone septa. Sample PCE levels were quantified via auto-injection into a gas chromatograph (Hewlett Packard Model 6890) equipped with an HP-624 column and electron capture detector. The practical range of detection for PCE in the model aquifer was from 0.5 to 80 mg/L. Samples observed to be above the upper detection limit were diluted in greater amounts of pentane in subsequent sampling events.

## 4. Results and Discussion

[20] PCE breakthrough at the transient observation point was used to determine when steady state transport behavior was achieved during pool dissolution. The observed behavior is plotted in Figure 3. The vertical lines in Figure 3 denote the synoptic sampling events (discussed below). The simulated transient portions of the breakthrough responses in Figure 3 are clearly less dispersed relative to the observed behavior. One possible source of this discrepancy is the effect of sorption. However, the primary (equilibrium) sorption effect is accounted for by the retardation factor. Thus, this discrepancy is most likely an artifact of the high sampling frequency (roughly every 15 min) and larger volumes (20–60 μL) required for analysis. This sampling regime drew the contaminant front forward, creating early breakthrough. The sampling also appeared to enhance dilution at the other end of the breakthrough curve such that a maximum concentration was not observed until the sampling frequency was markedly decreased. Sampling problems were less evident in the step-input tracer tests because the tritiated water could be analyzed with much lower sample withdrawals (2 μL). Thus, adjustment of the dispersion parameters to better simulate the front in Figure 3 would be inappropriate, and the values estimated via the tracer tests were used.

[21] The data in Figure 3 suggest that one to four days were needed for the dissolving pool to deliver a steady concentration roughly 73 cm downgradient from the pool. For reference, one day at a rate of 7.2 cm/h corresponds to about 2.5 pore volumes passing through this length of the

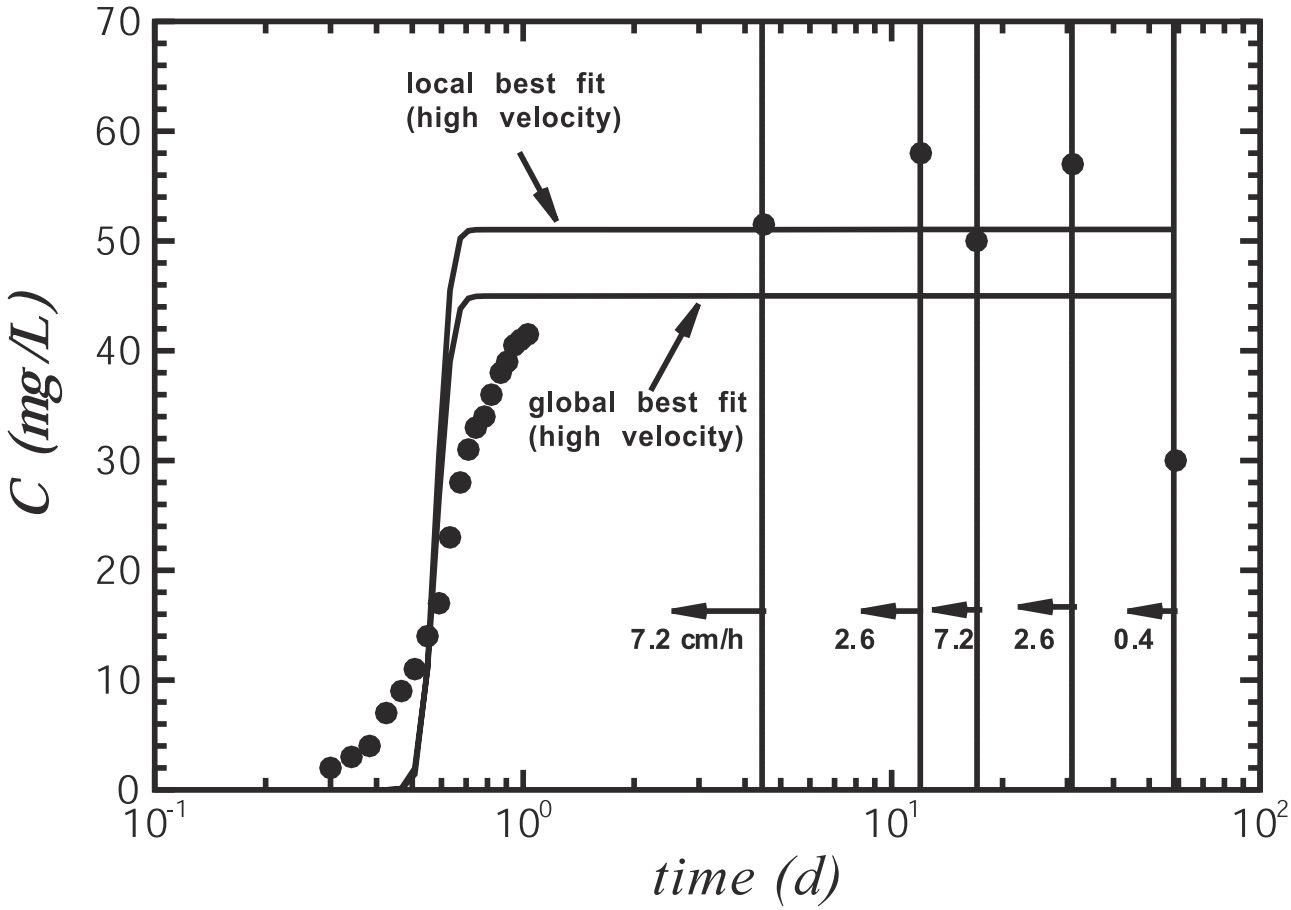


**Figure 3.** Observed and simulated PCE breakthrough behavior at the observation point roughly 73 cm downgradient from the pool (see sampling point designated in Figure 2). The solid lines describe the best fitting pool dissolution model simulations based on the independently estimated transport parameters with the globally optimized $k^*$ value (Table 1). The dashed line employs the same transport parameters with a locally optimized $k^*$ value. Vertical solid lines mark changes in the experimental flow rate.

model aquifer. The sampling-induced dispersion issue discussed above suggests that four days may be overestimating the time to steady state. Observations after five days demonstrate that a new steady state condition is achieved at the medium velocity, and that both the high and medium-velocity conditions were subsequently reproduced. This behavior confirms that mass loss from the finite pool had a minimal impact on the dissolution rate even after 31 days. The final datum was collected 28 days later at the low velocity (0.4 cm/h). This time corresponds to about 3.8 pore volumes passing between the pool and transient observation point, and was assumed to be sufficient to allow the new steady state to be achieved. However, a second sampling was not undertaken to confirm this notion. The glass-bottom experiment was terminated after 59 days.

[22] The simulations discussed throughout this section refer to those obtained using the pool dissolution model with the independently estimated parameters summarized in Table 1. The model fit to the observed data was optimized by adjusting the mass transfer coefficient ($k^*$) value via the PEST routine. For the local transient case, the fit was optimized for the data collected at the transient observation point exclusively. For each of the synoptic data sets, the $k^*$ value was fitted using the best, maximum and minimum dispersion coefficient estimates. Here, as in previous work [*Sciortino et al.*, 2000], the $k^*$ values were found to be more sensitive to the uncertainty associated with the dispersion parameters than to that associated with other transport parameters or with the observed concentrations. Thus the error bounds reported in Table 1 refer to the minimum $k^*$ estimates obtained using the maximum dispersion parameter estimates and the maximum $k^*$ estimates obtained using the minimum dispersion parameter estimates.

[23] In Figure 3, the local best fit (exclusively employing the transient data) is compared to the global best fit, based on the overall day-5 synoptic sampling results for a velocity of 7.2 cm/h. The discrepancy between the best estimates of the locally (0.24 cm/h) and globally (0.21 cm/h) optimized $k^*$ values was small. A comparison of the two fits indicates that the analytical model, despite its simplistic rendering of the pool shape, can be quite accurate when optimized to local observations. The simulation results are reasonable but less accurate at a given location with the globally optimized $k^*$ value.

[24] The observed and model-fitted synoptic behavior for the five velocities is summarized in Figures 4–6 The vertical proliferation of the dissolving pool was observed to be relatively weak as the concentration is seen to decrease from greater than 50% of PCE's solubility (roughly 100 mg/L) to less than 0.3% of solubility (0.5 mg/L, the practical detection

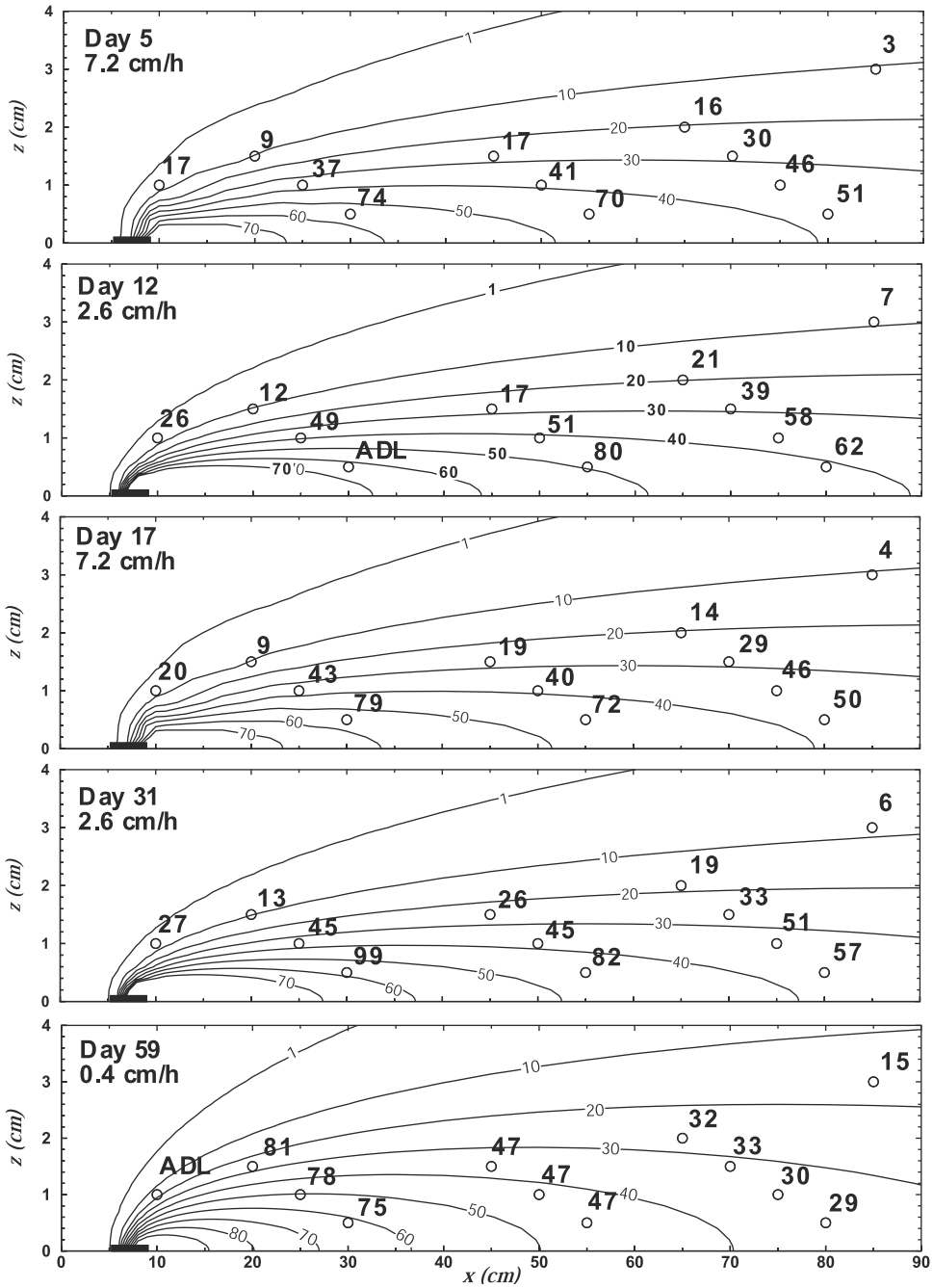


**Figure 4.** Simulated and observed PCE concentration profiles along the model aquifer centerline for the glass-bottom pool dissolution experiment (ADL and BDL are above and below method detection limit, respectively). The experimental sequence is from top to bottom for the sampling time (since pool placement) and interstitial velocities indicated.

limit) over a vertical distance of about 4 cm (Figure 4). The longitudinal limit of the plume was not observable over the length of this aquifer model. However, simulated plumes shown in Figure 4, extrapolated beyond the experimental domain (not shown), suggest that the concentrations were attenuated to 0.5 mg/L more than 200 cm away from the pool (roughly 50 pool diameters). The plumes attenuated sharply in the transverse horizontal direction, decreasing to low levels over distances of roughly 5 to 10 cm (one to several pool diameters), depending on the longitudinal location (see Figure 5).

[25] Figure 4 exhibits the plume profiles compiled from observations located along the aquifer centerline. Note the exaggerated vertical scale of these plots. The fine resolution of the observed data and appropriateness of the proposed model are especially evident in comparing the medium and high-velocity cases to the low-velocity case. For the medium and high-velocity cases, the results indicate that advection is sufficient to propagate the plume horizontally over the length-scale of this experimental aquifer. Thus, we observe a concentration that increases with depth despite the staggered observation points. This effect is also evident in

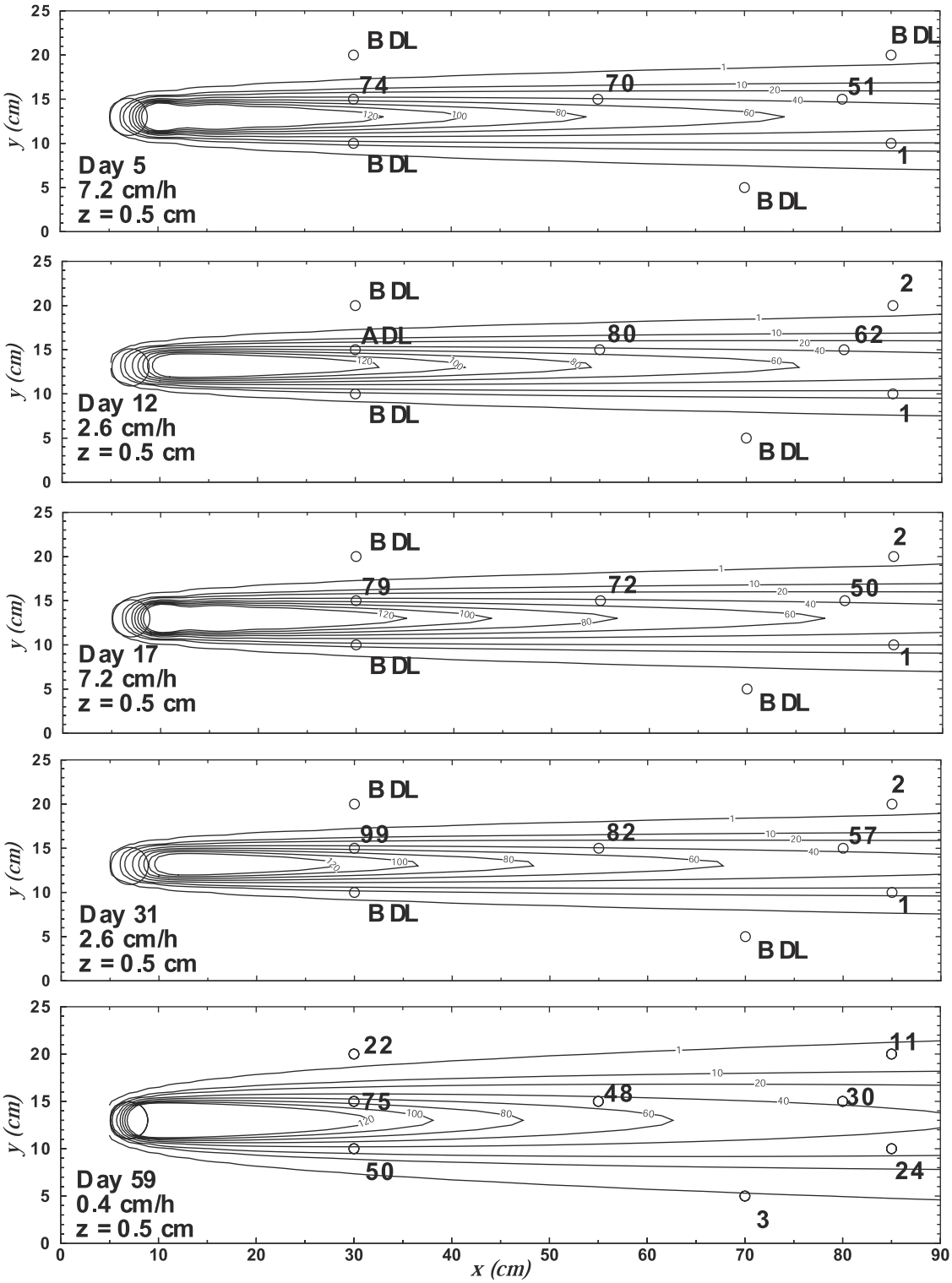


**Figure 5.** Plan view of simulated and observed PCE concentrations at elevation ($z$) 0.5 cm from the glass bottom (same experiment as Figure 4). The experimental sequence is from top to bottom for the sampling time (since pool placement) and interstitial velocities indicated.

the fact that observed concentrations generally increased after the change from the high to the medium velocity. For the low-velocity case, the plume failed to propagate as far in the horizontal direction, allowing for the accumulation of higher concentrations at many of the observation points. On the length-scale of this experiment, the overall effect was that the staggered observations tended toward constant values (tracking the isoconcentration lines). The dynamics described by these observations are captured well by the model fits based on the single adjustable parameter.

[26] Local discrepancies between simulated and observed profiles merit further discussion. The most prominent dis-

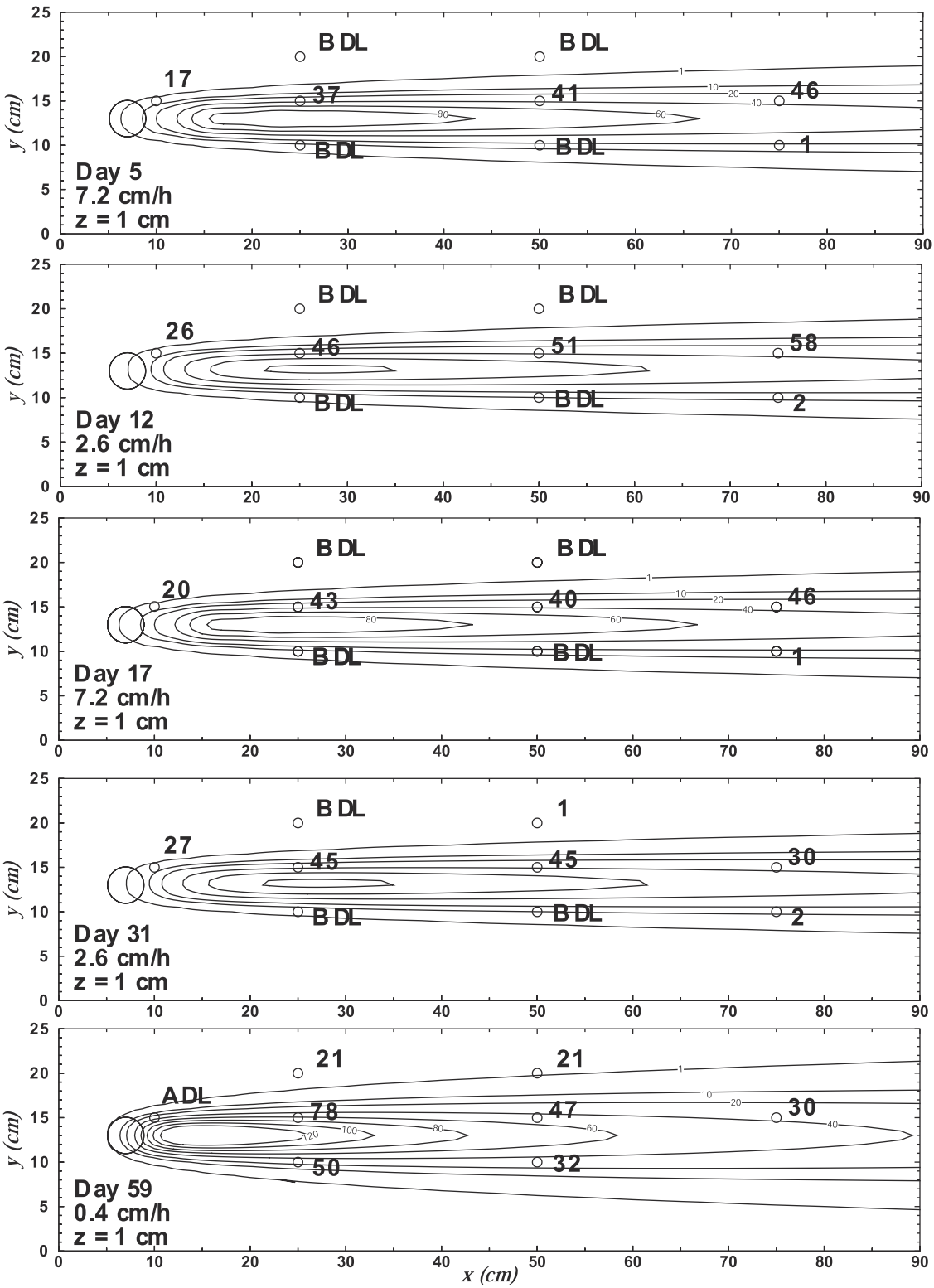


**Figure 6.** Plan view of simulated and observed PCE concentrations at elevation ($z$) 1.0 cm above the glass bottom (same experiment as Figure 4). The experimental sequence is from top to bottom for the sampling time (since pool placement) and interstitial velocities indicated.

crepancies for the medium and high velocities in Figure 4 are found at the lowermost observation points. For the low-velocity case, observation points near the pool are at odds with the model for all depths. One potential cause for this discrepancy is that the solubility value measured for this study was more than 20% lower than the 230 mg/L suggested by the data of *Imhoff et al.* [1997, Figure 3]. Using the greater value in the dissolution simulations resulted in slightly lower k* values. For example, inputting 230 mg/L for the medium-velocity case produced a revised k* value of

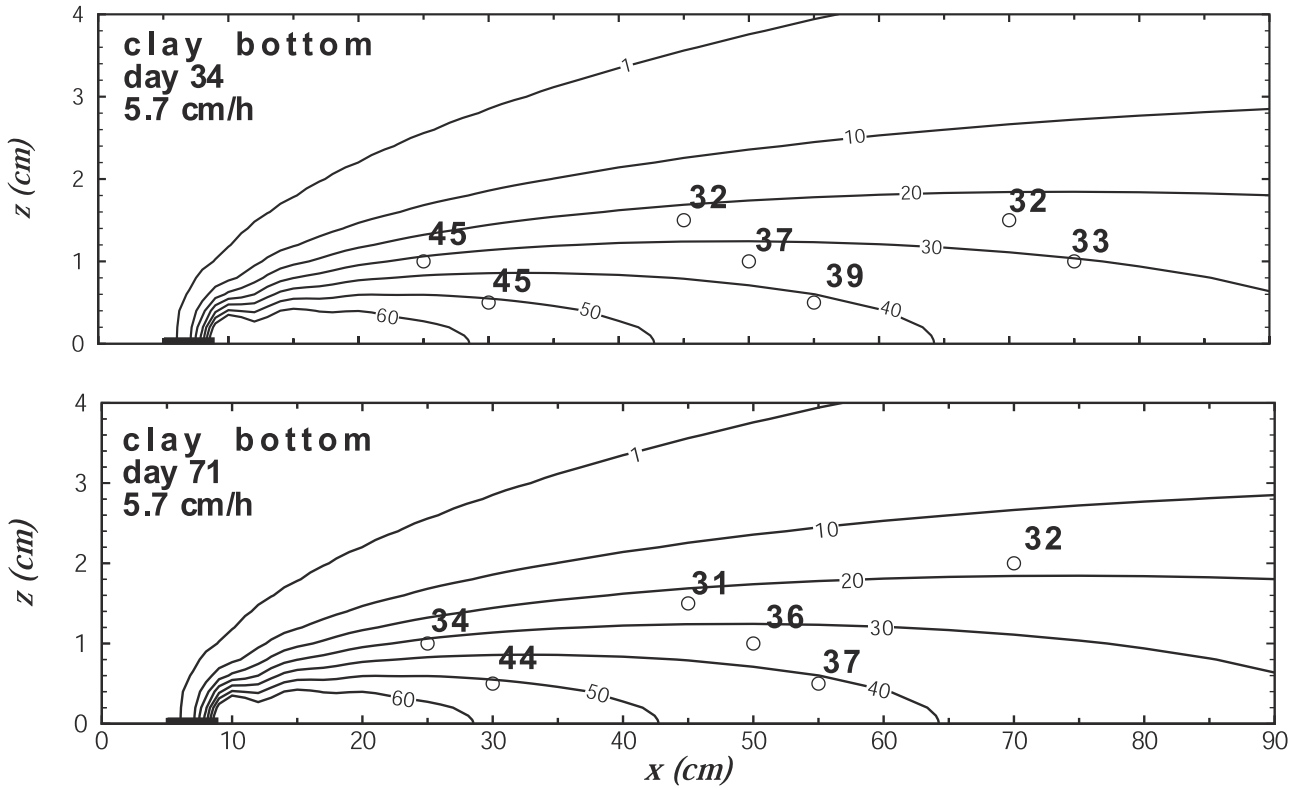


**Figure 7.** Simulated and observed PCE concentration profiles along the model aquifer centerline for the clay-bottom pool dissolution experiment. Elevations indicated are relative to the top of the clay layer.

0.19–0.20 cm/h (compared to 0.21–0.22 cm/h in Table 1). The quality of the fits was not improved as the revised simulations continued to fail to match at the near-pool and deep observation points. Thus, it was concluded that the solubility value measured here was sufficiently accurate. A more likely reason for the discrepancies appears to be associated with the difficulty in making accurate concentration measurements in regions associated with steep concentration gradients. This problem pertains to observation point installation, for horizontal and/or vertical deviations by as little as 1 mm from intended locations will result in significant sampling errors in regions of steep gradient. A potentially more significant problem is inherent in modeling an irregularly shaped pool using the analytical model for the average (circular) pool shape (see pool rendering in Figure 1b). Sampling points downgradient of pool diameters greater than the average feel a stronger source than other regions; those downgradient of less-than-average diameters feel a weaker source. Simulations allowing for the adjustment of both dispersion coefficients and $k^*$ values improved the quality of the simulation at near-pool and low elevation sampling points, but at the expense of the more numerous elevated observations. Given the potential problems associated with sampling at these locations, the fitting exercises were repeated while omitting these data. The mass transfer coefficient estimates were found to be insensitive to the presence or absence of these data. This result is not surprising given the large number of observations used in fitting exercises (see footnote to Table 1).

[27] Figures 5 and 6 exhibit planar views of the same plumes at elevations of 0.5 and 1.0 cm, respectively, above the glass bottom. Agreement between the model and observed concentrations is poor for the lower elevation for all cases but the low velocity. This is not surprising given that the centerline observations for these data sets are the same as those used to develop the profiles in Figure 4. At the 1-cm elevation, there is good agreement between the model and the observed concentrations. The system dynamics discussed above are just as apparent from a planar perspective, as the centerline concentrations are reasonably constant longitudinally for the medium and high velocities, but decrease longitudinally for the low-velocity case. Again, the dissolution model results are in accord with this behavior.

[28] Observation point density was insufficient to quantify transverse horizontal plume expanse conclusively in most cases. Nonquantifiable traces were observed along the plume edges, suggesting that the simulated plumes in Figures 5 and 6 represent a reasonable estimate of the plume width for the medium- and high-velocity cases. However, the low-velocity case indicates that the plume is substantially wider than the best fitting simulation would indicate. Closer inspection of the off-centerline low-velocity observations ($y$ = 10 cm and $y$ = 20 cm) also confirms a degree of asymmetry in observed plume favoring the side "above" the centerline (y = 20 cm). This result is indicative of the irregular pool shape (Figure 1b), which may have contributed a stronger mass flux on this side of the system.

[29] The clay-bottom experiment yielded the data shown in the concentration profiles in Figure 7. The amount of data available for analysis was limited by the narrow horizontal extent of the plumes emanating from this pool, and by the

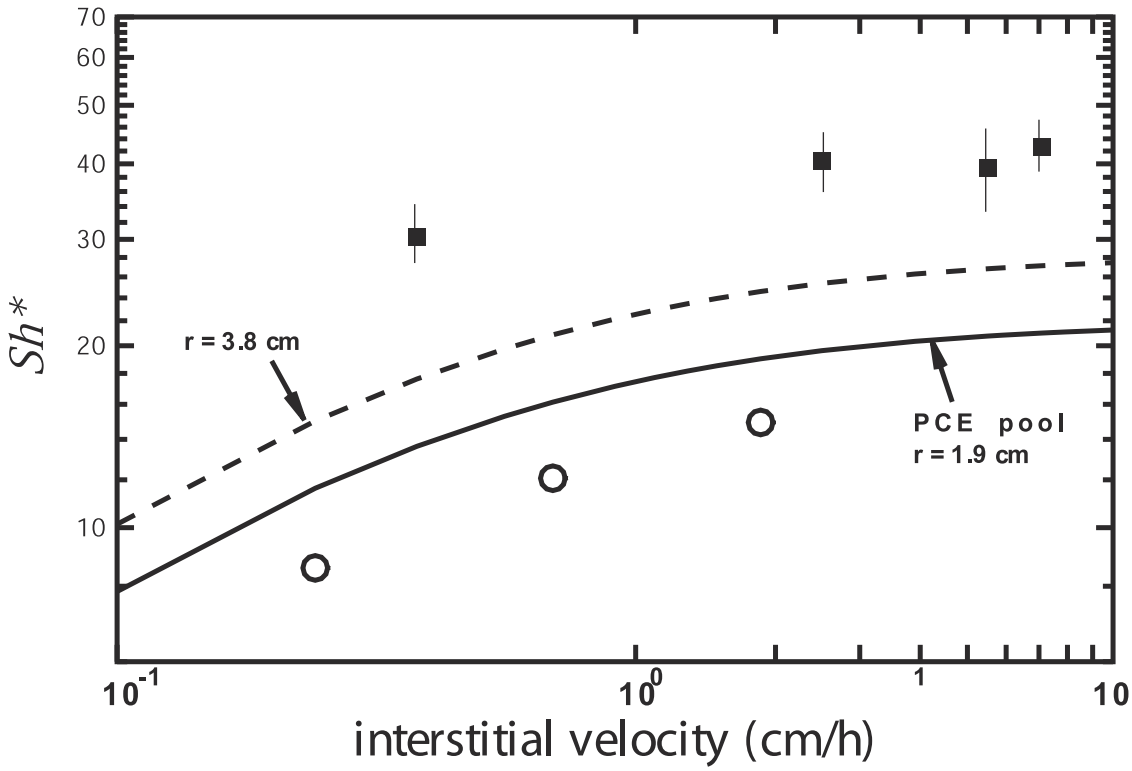


**Figure 8.** Observed (squares, this work, open circles, *Chrysikopoulos et al.* [2000]) and correlation-predicted (equation (10)) modified Sherwood numbers ($Sh^*$) as a function of the interstitial velocity ($U_x$). Solid line represents the correlation prediction for the independent parameter estimates of this study while the dashed lines correspond to correlation predictions with artificially increased pool surface area values. The error bars on the experimentally based $k^*$ values bound the range determined by fitting this parameter subject to the minimum and maximum dispersion parameter estimates.

occurrence of needle-clogging (due to particle intrusion during sampling). The model fits to the two data sets yielded similar $k^*$ values that were consistent with those obtained from the glass-bottom experiments at the high velocity. In contrast to the high-velocity glass-bottom results, the 0.5-cm elevation clay-bottom observations were slightly less than best fitting simulation would dictate. This finding suggests that diffusion of the aqueous PCE into the adjacent clay layer may have played a role. However, the lag-time prior to sampling in the clay-bottom experiment was intended to allow for this behavior. Furthermore, the discrepancy between the model and the simulation in these locations is relatively minor. These points suggest that the two media were nearly in equilibrium by the time sampling occurred.

## 5. Pool Mass Depletion Estimates

[30] Using the estimated mass transfer coefficients it is possible to estimate the mass flux from the pool using Fick's first law as expressed in equation (6). The overall mass loss from the pool can then be estimated as the product of the flux and the pool area:

$$\frac{dM}{dt} = -k^* C_s A \tag{9}$$

where $M$ is the mass of PCE in the pool and $A$ is the pool's surface area. Integrating equation (9) over the course of the experiments and accounting for the different $k^*$ values at the different velocities yields mass losses of about 0.5 g over 51 days and 0.7 g over 71 days for the glass- and clay-bottom experiments, respectively. These losses correspond to about 31% and 43% of the initial pool masses. Given that the stationary nature of the plumes was confirmed for all but the low-velocity experiment (which corresponded to about 4 additional pore volumes beyond the termination of the second medium-velocity experiment), it was concluded that the corresponding change in pool shape and interfacial area was insufficient to markedly alter the dissolution rate.

## 6. Correlating Mass Transfer Behavior with Hydrodynamic Conditions

[31] In Figure 8, the dimensionless mass transfer behavior is summarized in terms of the modified Sherwood number ($Sh^* = k^* l_c / D_e$), where the characteristic length ($l_c$) employed here is the square root of the pool area [*Kim and Chrysikopoulos*, 1999]. Results based on the mass transfer coefficients estimated in this work are compared to those estimated using an ideally configured pool [*Chrysikopoulos et al.*, 2000] and to those predicted by the following theoretical mass transfer correlation from *Kim and Chrysikopoulos* [1999]:

$$Sh^* = 1.74 \left(Pe_x^*\right)^{0.33} \left(Pe_y^*\right)^{0.4} \tag{10}$$

where $Pe_x^*(= U_x r_p / D_x)$ and $Pe_y^*(= U_x r_p / D_y)$ are the Peclet numbers for a circular pool in the $x$ and $y$ directions (see

Table 1 for Peclet number estimates). The *Sh** values estimated here are two to three times greater than those predicted by the correlation parameterized by the best fitting values for this work, and roughly three to four times greater than those estimated in the previous study of an ideally configured pool.

[32] The relatively large discrepancy between the *Sh** values observed in this work and those from the previous investigations may be due in part to experimental errors of the type mentioned previously (e.g., sampling point misalignment, and the idealized pool configuration assumed by the analytical model). Another possible error source not discussed previously could be localized vertical velocity components and the associated enhancement of the dispersivity in the vicinity of a DNAPL-impacted zone [*Pennell et al.*, 1993]. These types of effects are not accounted for in this work and their presence would also bias results toward greater Sh* values.

[33] More important than experimental errors discussed above are the limitations imposed by the ideally shaped pool modeling assumptions. Whenever a pool develops in a porous medium, pore level effects will tend to increase the interfacial area relative to the smooth approximation. Larger scale interfacial effects are evident in the deviation from circular behavior seen in Figure 1b. The present model will tend to overestimate the mass transfer coefficient in an effort to compensate for the underestimated surface area. Specific interfacial areas calculated for residual DNAPL using pore network models range from about 0.3 to 2 $mm^2/mm^3$ [*Held and Celia*, 2001b]. Estimating our effective porous medium volume as the observed pool area (11.3 $cm^2$) multiplied by the pool thickness (estimated as DNAPL volume injected (1 mL) divided by (the pool area times the porosity)) and multiplying this overall volume by 2 $mm^2/mm^3$ yields an $A_{nw}$ value for the pool of 12 $cm^2$, very similar to the smooth pool approximation of 11.3 $cm^2$. Assuming that the pool is thicker, say 1 mm in the extreme, the resulting $A_{nw}$ estimate for the pool increases to 24 $cm^2$. Thus the pore scale effects may be significant here, but the larger scale effects causing the noncircular pool shape appear to be equally or more important in this system.

## 7. Summary and Conclusions

[34] Aqueous plumes emanating from realistic DNAPL pools placed atop glass and clay aquifer-bottoms were monitored at downgradient sampling points. All required transport parameters, with the exception of the pool-average mass transfer coefficient ($k^*$), were estimated independently. With adjustment of the average mass transfer coefficient value, the analytical solution for pool dissolution in a homogeneous porous medium was found to adequately describe the observed PCE plume. Specific conclusions stemming from this work are as follows.

1. Despite the finite pool volume (1 mL), observed plumes achieved a quasi-steady state distribution over extended time periods (months). A relatively constant mass flux developed at the pool-groundwater interface acting as the plume source. This flux was sufficiently slow that the effect of mass loss on pool geometry (effective dissolution surface) was minimal over the course of these experiments. Thus, it appears that pool-water interfacial areas change on a slower timescale than do residual-water interfacial areas.

2. Pool dissolution behavior was reasonably well-modeled using boundary layer theory (second type boundary condition) assuming a simplistic (circular) pool shape. The model was especially successful in simulating the vertical and longitudinal concentration profile near the centerline of the plume. However, local discrepancies between the model and observations were significant, especially near the pool. These discrepancies may be the result of pore scale surface curvature and larger scale shape irregularities that could not be simulated using the present model.

3. Estimated mass transfer coefficient ($k^*$) values were two to three times greater than values predicted by a theoretically based mass transfer correlation for elliptical/circular pools and three to four times greater than those estimated in a dissolution study involving an ideally configured pool. The most likely cause of these discrepancies was the pool dissolution model's failure to address interfacial issues associated with the emplaced pool and overcompensation in the form of elevated mass transfer coefficients.

[35] The rates and steady contaminant distributions summarized here should be useful to contaminant hydrogeologists in search of more accurate source depictions for larger-scale transport models. For example, it is likely that alternative boundary conditions (first- and third-type) can be used to adequately model the pool dissolution process. The appropriate conditions and parameters under which alternative boundary conditions are valid need to be identified. Additional future research aimed at elucidating the connection between pool dissolution and pore-scale mechanisms defining the pool-water interface is clearly warranted. Such work will become increasingly complicated in heterogeneous porous media.

[36] **Acknowledgments.** This work was supported by a grant from the U.S. Environmental Protection Agency's Office of Exploratory Research (award R-823579-01-0). The content of this manuscript has not been subjected to the Agency's review and no official endorsement should be inferred. The authors thank Priti Brahma for measuring PCE solubility at the temperature of the study.

## References

Anderson, M. R., R. L. Johnson, and J. F. Pankow, Dissolution of dense chlorinated solvents into ground-water, 1, Dissolution from a well-defined residual source, *Ground Water*, *30*(2), 250–256, 1992.

Ball, W. P., and P. V. Roberts, Long-term sorption of halogenated organic chemicals by aquifer material, 1, Equilibrium, *Environ. Sci. Technol.*, *25*(7), 1223–1237, 1991.

Bear, J., *Dynamics of Flow in Porous Media*, Elsevier Sci., New York, 1972.

Chrysikopoulos, C. V., Three-dimensional analytical models of contaminant transport from nonaqueous phase liquid pool dissolution in saturated subsurface formations, *Water Resour. Res.*, *31*(4), 1137–1145, 1995.

Chrysikopoulos, C. V., and T.-J. Kim, Local mass transfer correlations for non-aqueous phase liquid pool dissolution in saturated porous media, *Transp. Porous Media*, *38*(1/2), 167–187, 2000.

Chrysikopoulos, C. V., and K. Y. Lee, Contaminant transport resulting from multicomponent nonaqueous phase liquid pool dissolution in three-dimensional subsurface formations, *J. Contam. Hydrol.*, *31*(1–2), 1–21, 1998.

Chrysikopoulos, C. V., E. A. Voudrias, and M. M. Fyrillas, Modeling of contaminant transport resulting from dissolution of nonaqueous phase liquid pools in saturated porous media, *Transp. Porous Media*, *16*(2), 125–145, 1994.

Chrysikopoulos, C. V., K. Y. Lee, and T. C. Harmon, Dissolution of a well-defined trichloroethylene pool in saturated porous media: Experimental design and aquifer characterization, *Water Resour. Res.*, *36*(7), 1687–1696, 2000.

Crank, J., *The Mathematics of Diffusion*, Oxford Univ. Press, New York, 1975.

Dela Barre, B. K., Mass transfer coefficient estimation for dense nonaqueous phase liquid pool dissolution using a three-dimensional physical aquifer model, Ph.D. dissertation, 118 pp., Univ. of Calif., Los Angeles, 1999.

Doherty, J., L. Brebber, and P. Whyte, PEST: Model-independent parameter estimation, Watermark Computing, Brisbane, Australia, 1994.

Harmon, T. C., and P. V. Roberts, A comparison of intraparticle sorption and desorption rates for a halogenated alkene in a sandy aquifer material, *Environ. Sci. Technol.*, *28*(9), 1650–1660, 1994.

Held, R. J., and M. A. Celia, Pore-scale modeling and upscaling of nonaqueous phase liquid mass transfer, *Water Resour. Res.*, *37*(3), 539–549, 2001a.

Held, R. J., and M. A. Celia, Modeling support of functional relationships between capillary pressure, saturation, interfacial area and common lines, *Adv. Water Res.*, *24*, 325–343, 2001b.

Holman, H. Y. N., and I. Javandel, Evaluation of transient dissolution of slightly water-soluble compounds from a light nonaqueous phase liquid pool, *Water Resour. Res.*, *32*(4), 915–923, 1996.

Imhoff, P. T., A. Frizzell, and C. T. Miller, Evaluation of the thermal effects on the dissolution of a nonaqueous phase liquid in porous media, *Environ. Sci. Technol.*, *31*, 1615–1622, 1997.

Jia, C., K. Shing, and Y. C. Yortsos, Visualization and simulation of NAPL solubilization in pore networks, *J. Contam. Hydrol.*, *35*, 363–387, 1999a.

Jia, C., K. Shing, and Y. C. Yortsos, Advective mass transfer from stationary sources in porous media, *Water Resour. Res.*, *35*(11), 3239–3251, 1999b.

Johnson, R. L., and J. F. Pankow, Dissolution of dense chlorinated solvents into groundwater, 2, Source functions for pools of solvent, *Environ. Sci. Technol.*, *26*(5), 896–901, 1992.

Khachikian, C. S., and T. C. Harmon, Nonaqueous phase liquid dissolution in porous media: Current state of knowledge and research needs, *Transp. Porous Media*, *38*(1/2), 3–28, 2000.

Kim, T.-J., and C. V. Chrysikopoulos, Mass transfer correlations for nonaqueous phase liquid pool dissolution in saturated porous media, *Water Resour. Res.*, *35*(2), 449–459, 1999.

Lee, K. Y., and C. V. Chrysikopoulos, NAPL pool dissolution in stratified and anisotropic porous formations, *J. Environ. Eng.*, *124*(9), 851–862, 1998.

Marquardt, D. W., Solution of nonlinear chemical engineering models, *Chem. Eng. Progr.*, *55*(6), 65–70, 1959.

Marquardt, D. W., An algorithm for least-squares estimation of nonlinear parameters, *J. Soc. Indust. Appl. Math.*, *11*(2), 431–441, 1963.

Miller, C. T., G. Christakos, P. T. Imhoff, J. F. McBride, J. A. Pedit, and J. A. Trangenstein, Multiphase flow and transport modeling in heterogeneous media: Challenges and approaches, *Adv. Water Res.*, *21*(2), 77–120, 1998.

Pearce, A. E., E. A. Voudrias, and M. P. Whelan, Dissolution of TCE and TCA pools in saturated subsurface systems, *J. Environ. Eng.*, *120*(5), 1191–1206, 1994.

Pennell, K. D., L. M. Abriola, and W. J. Weber, Surfactant-enhanced solubilization of residual dodecane in soil columns, 1, Experimental investigation, *Environ. Sci. Technol.*, *27*(12), 2332–2340, 1993.

Perkins, T. K., and O. C. Johnston, A review of diffusion and dispersion in porous media, *Soc. Pet. Eng. J.*, *3*, 70–80, 1963.

Pfannkuch, H. O., Determination of the contaminant source strength from mass exchange processes at the petroleum-ground-water interface in shallow aquifer systems, paper presented at the NWWA Conference on Petroleum Hydrocarbons and Organic Chemicals in Ground Water, Natl. Well Water Assoc., Dublin, Ohio, 1984.

Powers, S. E., C. O. Loureiro, L. M. Abriola, and W. J. Weber, Theoretical study of the significance of nonequilibrium dissolution of nonaqueous phase liquid in subsurface systems, *Water Resour. Res.*, *27*(4), 463–477, 1991.

Reeves, P. C., and M. A. Celia, A functional relationship between capillary pressure, saturation, and interfacial area as revealed by a pore-scale network model, *Water Resour. Res.*, *32*(8), 2345–2358, 1996.

Saba, T., and T. H. Illangasekare, Effect of groundwater flow dimensionality on mass transfer from entrapped nonaqueous phase liquid contaminants, *Water Resour. Res.*, *36*(4), 971–979, 2000.

Schaefer, C. E., D. E. DiCarlo, and M. J. Blunt, Determination of water-oil interfacial area during three-phase gravity drainage in porous media, *J. Colloid Interface Sci.*, *221*, 308–312, 2000.

Sciortino, A., T. C. Harmon, and W. W.-G. Yeh, Inverse modeling for locating dense nonaqueous pools in groundwater under steady flow conditions, *Water Resour. Res.*, *36*(7), 1723–1736, 2000.

Voudrias, E. A., and M. F. Yeh, Dissolution of a toluene pool under constant and variable hydraulic gradients with implications for aquifer remediation, *Ground Water*, *32*(2), 305–311, 1994.

Whelan, M. P., E. A. Voudrias, and A. E. Pearce, DNAPL pool dissolution in saturated porous media—Procedure development and preliminary results, *J. Contam. Hydrol.*, *15*(3), 223–237, 1994.

Wilke, C. R., and P. C. Chang, Correlation of diffusion coefficients in dilute solutions, *AIChE J.*, *1*, 264–270, 1955.

Zhou, D., L. A. Dillard, and M. J. Blunt, A physically based model of dissolution of nonaqueous phase liquids in the saturated zone, *Transp. Porous Media*, *39*, 227–255, 2000.

C. V. Chrysikopoulos, Department of Civil and Environmental Engineering, University of California, Irvine, CA 92697-2175, USA.

B. K. Dela Barre, Tetra Tech EM Inc., 1325 Automotive Way, Suite 200, Reno, NV 89502, USA.

T. C. Harmon, Department of Civil and Environmental Engineering, University of California, 5732 Boelter Hall, Los Angeles, CA 90095-1593, USA. (tharmon@ucla.edu)